Available online at www.eccomasproceedia.org
Eccomas Proceedia COMPDYN (2023) 1644-1659

ECCOMAS
Proceedia

COMPDYN 2023
9th ECCOMAS Thematic Conference on
Computational Methods in Structural Dynamics and Earthquake Engineering
M. Papadrakakis, M. Fragiadakis (eds.)
Athens, Greece, 12-14 June 2023

# SEISMIC VULNERABILITY ASSESSMENT OF VAULTED MAYA CONCRETE TEMPLES IN BONAMPAK, CHIAPAS, MÉXICO

**Humfrey M. Kimanya, Anna M. Remus, Omar Hamad, Justin W. Sennyondo, Dung T. Nguyen, Selman Tezcan and Renato L. Perucchio**

Department of Mechanical Engineering, University of Rochester, Rochester, NY 14611, USA

e-mail: hkimanya@u.rochester.edu, aremus2@u.rochester.edu, ohamad@u.rochester.edu, jsennyon@u.rochester.edu, dnguy23@u.rochester.edu, stezcan@ur.rochester.edu, rlp@me.rochester.edu

## Abstract

*Vaulted concrete structures at the Late Classic Maya complex of Bonampak, Chiapas, Mexico (circa AD. 580-800) house some of Mexico's best-preserved Maya murals, but they are at risk due to significant seismic hazard in the region. Seismic vulnerability assessments of these structures via pushover analysis of 3D, nonlinear, finite element (FE) models provide insight into structural collapse mechanisms under unilateral acceleration. A sensitivity analysis of lateral capacity based on tensile strength of Maya concrete, foundation inclination, and the presence/absence of crestería (roof combs) is performed using Abaqus/CAE Explicit. The concrete damaged plasticity (CDP) formulation is implemented with parameters derived from experimental studies of Maya lime mortar and concrete from Maya historical sites near Bonampak. Structural collapse is detected from an analysis of the time-evolution of plastic dissipation, strain, and kinetic energies and basal reactions. The present work continues investigation of Structure 3 and adds analysis of Structure 1 under monotonically increasing lateral acceleration in the EW and NS direction. Both structures in their current states are found to be more vulnerable under loading in the NS than EW direction. The minimum obtained lateral capacities from applied NS acceleration of 0.55g for Structure 1 and 0.80g for Structure 3 imply that kinematic limit analyses using 2D rigid-body sectional models substantially overestimate seismic vulnerability due to (a) assuming zero tensile strength of Maya concrete and (b) ignoring the actual 3D architecture of the temples. Determining the extent to which intervention is necessary is one of the major challenges for preserving historical masonry structures. This research offers one example of how 3D nonlinear FE models may help avoid unnecessary interventions.*

**Keywords:** nonlinear finite element analysis, pushover analysis, concrete damaged plasticity, Maya concrete, lateral capacity, peak ground acceleration.

ISSN:2623-3347 
Peer-review under responsibility of the organizing committee of COMPDYN 2023.
doi: 10.7712/120123.10508.20489

# 1 INTRODUCTION

## 1.1 Background

The archaeological site Bonampak is a complex of Maya temples. Academic research on them began in the 1940s, and the site is renowned for the well-preserved murals found in its largest standing building, Structure 1. In terms of architecture, art motifs, and hieroglyphs on stelae, Bonampak shares many features with neighboring archaeological sites. Accordingly, Bonampak is believed to be one city in a culturally uniform Maya region under the influence of Yaxchilan: a larger, politically-dominating city located 20 km north of Bonampak [1].

Figure 1: Murals from inside Structure 1 [2].

The buildings at Bonampak are small, one-story constructions characterized by thick corbelled vaults. Their walls are built using roughly shaped, flat, limestone blocks resting on beds of lime mortar. Partially collapsed vaults reveal larger flat stones used for facing the intrados, smaller stones at the extrados, and lime-based concrete filling the interior of the vault.

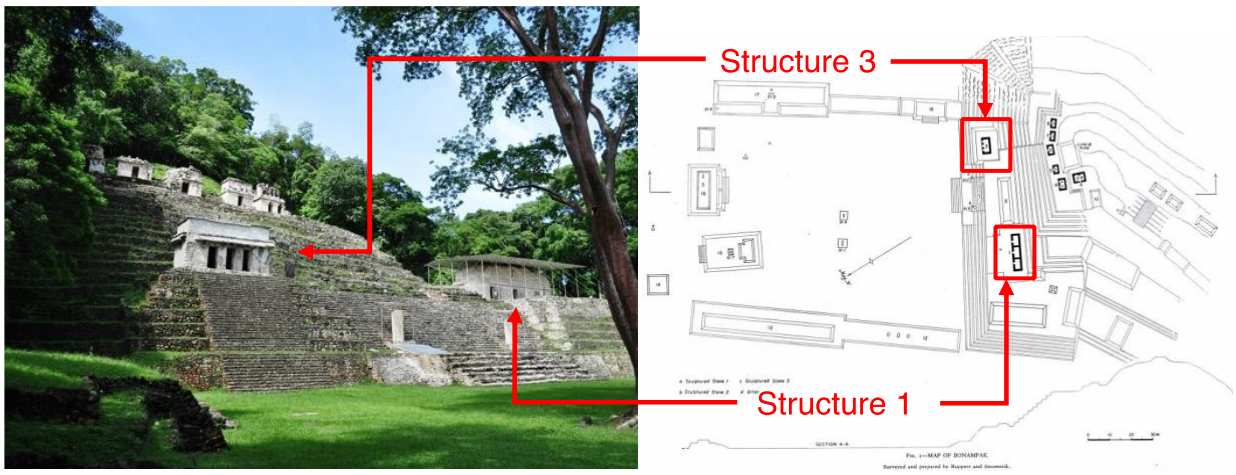


Figure 2: Structure 3 (left) and Structure 1 (right), with corresponding plan view (adapted from [1]).

Structures 1 and 3 are constructed on earth-filled terraces. Their structurally intact vaults suggest that they are in a good state of preservation. Structure 1 is comprised of three rooms separated by thick masonry walls. Each room has an entrance to the exterior of the building. The building also presents stucco decorations on its exterior facade. Structure 3 has a single room with three doorways separated by columns. On its roof, Structure 3 shows stone

protrusions (Figure 3, left), suggesting that the temple was adorned with a feature called *crestería*, or "roof comb." This ornamental structure is common in Maya architecture [3].

Figure 3: Inclined base of Structure 3 puts this and other buildings at the complex at higher risk [4],[5].

In the 1940s, Bonampak was documented with architectural and archaeological surveys and photographic collections [5]. The elevation drawings of Structure 1 and Structure 3, the objects of the present work, record fractures and parts of the roofs completely collapsed (Figure 3). The entirety of Structure 3 was documented as leaning northwards on its platform. Eventually, the structures were consolidated by the *Instituto Nacional de Antropología e Historia* (INAH) of Mexico, an organization that has led many preservation projects at the Bonampak site and continues such efforts to this day.

## 1.2 Motivation & Objectives

The Bonampak complex is located in Chiapas, Mexico, a seismically active region exhibiting complex tectonics and crustal deformation (Figure 4) [6]. Since the Bonampak structures rest near steep stairways on artificial terraces, and Structure 3 experiences a foundation inclination, the temples are at an increased risk of structural damage in the event of seismic activity. The focus of present research is on Structures 1 and 3. Both structures house valuable murals and decorations (e.g., ornamental reliefs) which are important to the study of Maya history and culture. The loss of these assets due to possible damage to the structures will prove costly.

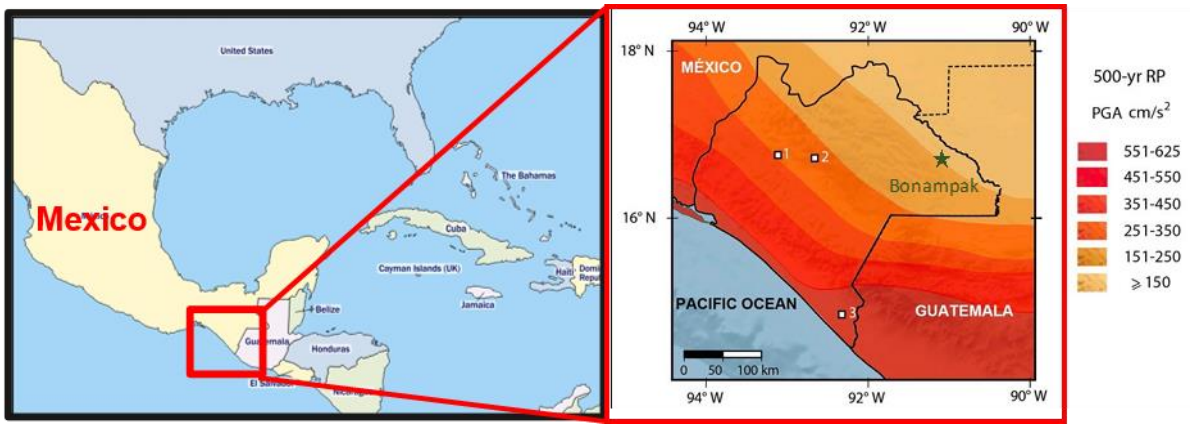


Figure 4: Geographic location of Bonampak Temple [7].

The structural behavior of the buildings under seismic conditions was recently investigated by Flores and Orea from INAH using kinematic limit analysis [6]. They noted that the structures developed fissures after an earthquake in 2005, and that Structure 3 currently exhibits an average downward tilt of 6° oriented northeast. We conducted additional research on Structure 3 using 3D FEA to further determine its vulnerability to seismic risks and sensitivity to tensile strength of Maya concrete [8]. It was found that the structure is safe from collapse under seismic movement within the seismic demand of the Chiapas region.

The present study aims to expand our earlier research and determine and compare the lateral capacities for Structures 1 and 3 and to identify factors affecting these capacities. Understanding the possible failure mechanisms through analysis of these structures in 3D allows us to assess the future risks the buildings may face and the necessity (or lack thereof) of structural preservation interventions.

In this paper, we specifically investigate the sensitivity of the temples' structural response to (a) the tilted base, (b) the possible presence and collapse of crestería, and (c) the assumed tensile strengths of Maya concrete. We compare the differences between the models of Structure 1 and 3, and the seismic demand of the Bonampak area. The seismic demand is obtained from Peak Ground Acceleration (PGA) data, which is the maximum ground acceleration recorded in the last 500 years (Figure 4). Towards these ends, we characterize the behavior of Maya concrete using the Concrete Damaged Plasticity (CDP) formulation, and we construct 3D nonlinear finite element (FE) models to be analyzed using Abaqus/CAE Explicit [9].

## 2 MODELLING AND SIMULATION

### 2.1 Geometry

Structures 1 and 3 are modelled based on both architectural surveys of Bonampak [1] and former research done in the area [6]. The geometry of both structures is shown in Figure 5**,** below. The dimensions shown are of frontal and side views. The structures, which in reality have subtle asymmetries, are idealized to be symmetric for easier modeling. Structure 1 does not appear to have had a crestería and is approximately twice as long as Structure 3.

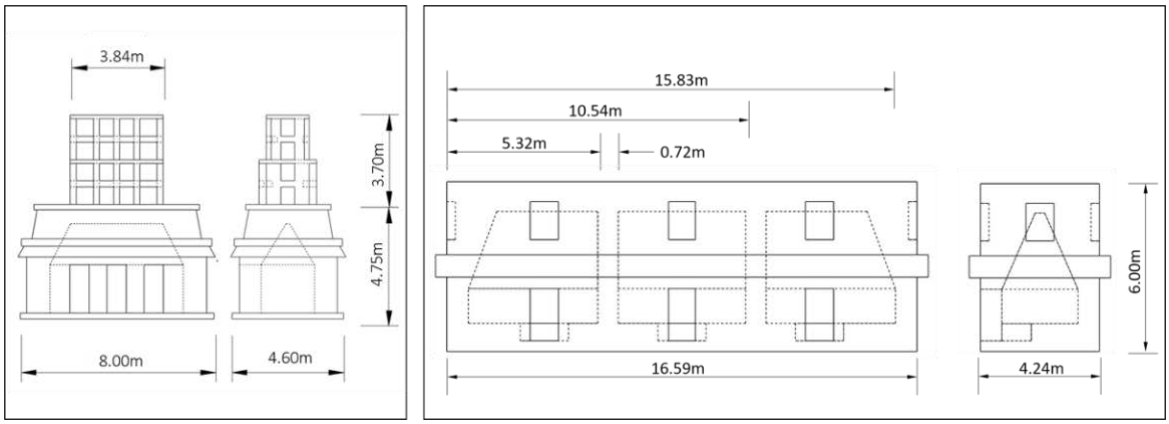


Figure 5: Geometry of Structure 3 (left) and Structure 1 (right). The two structures are out of scale.

The crestería in Structure 3 is reconstructed based on the surviving crestería of Structure 4 in the Bonampak complex, and it is consistent with the general trends in Maya architecture [1]. The present reconstruction is based on similar investigation done in previous work [1][6]. Figure 6 illustrates the 3D models as they are implemented in Abaqus/CAE Explicit [9].

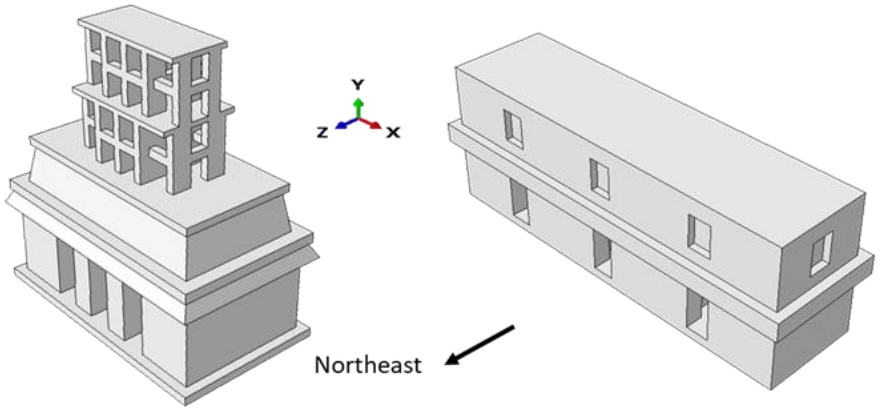


Figure 6: 3D layout for Structure 3 (left) and Structure 1 (right). The two structures are out of scale.

## 2.2 Boundary conditions, loading, and mesh

In real life, the structures are built onto man-made terraces, but for this analysis they are modelled with a fully constrained base, simulating full fixation to the ground. This is a reasonable assumption given that we wish to compare these results with the work of Flores and Orea [6]. They identified an inclination of 6° at the base of Structure 3, but Structure 1 does not indicate any inclination.

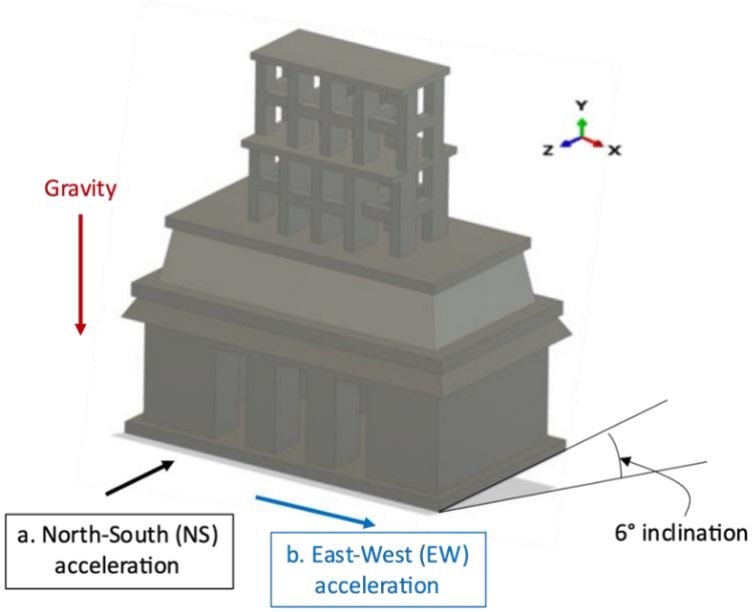


Figure 7: Loading and boundary conditions for Structure 3.

We implement a pushover analysis method which involves applying a monotonically increasing lateral acceleration applied directly to the ground until failure [10]. Pushover analysis is conducted for Structure 3 and Structure 1 using two steps and is illustrated with Structure 3 in Figure 7. Gravity is applied as a linearly increasing ramp for the first 10 seconds of the analysis using a quasi-static approach. In the second step of the analysis, the fully fixed boundary condition is disabled to allow unilateral acceleration to be applied in a specific direction at the base; in other directions, displacement constraints are used. Acceleration is

applied as a linearly increasing ramp for 10 seconds. Simulations were run with either North-South (NS) or East-West (EW) acceleration (Figure 7). The total analysis time is 20 seconds.

Both structures are meshed using quadratic tetrahedral elements (C3D10M). Global seeding is 0.4 m. Seeding corresponds to the size of individual tetrahedral elements. Since the crestería contains dimensions for its pillars that are less than 0.4 m, localized seeding of 0.25 m is used to refine the mesh for these more complex features (Figure 8). These choices improve the mesh quality and optimize the run time of the analyses.

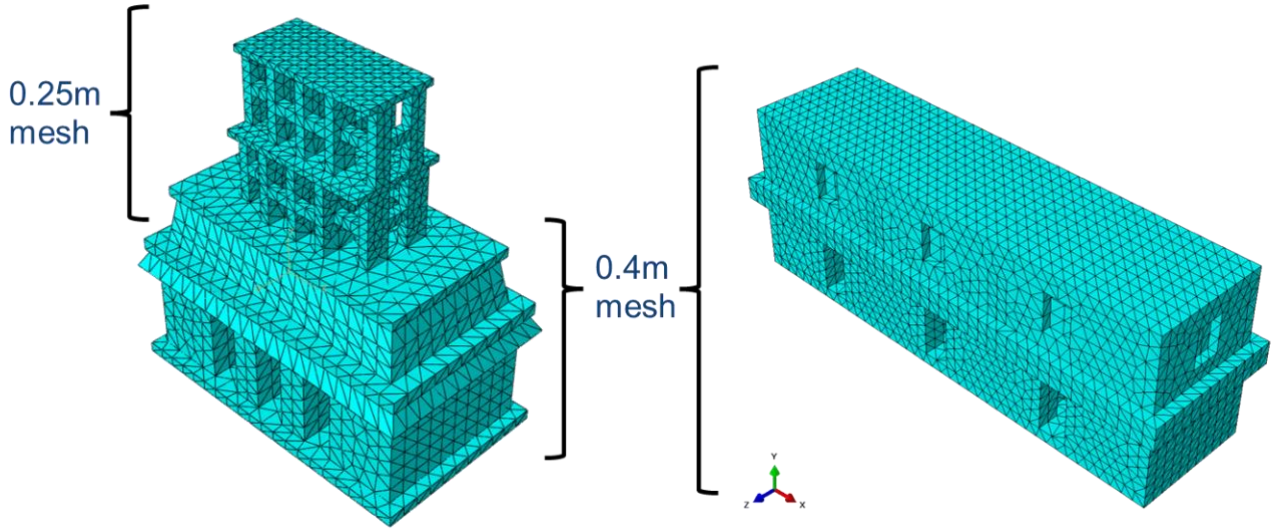


Figure 8: Mesh and mesh seeding dimensions for Structure 3 (left) and Structure 1 (right).

## 2.3 Materials

The material properties used for Maya concrete characterization are established based on masonry modeling methods [11] applied to available data on concrete from neighboring Maya sites. These were obtained from published literature of experimental studies of concrete that came from Yaxchilan and Palenque [12], [13]. The derived values are summarized in Table 1 and Figure 9.

We compute average values for density and compressive strength based on three Yaxchilan concrete samples tested in simple compression [13]. Different testing on Yaxchilan concrete produced the only available measure of an elastic modulus [12]. One published tensile strength of Yaxchilan concrete, 1.8 MPa, is unrealistically high [1]. Thus, we adopt the recommendations of Angelillo et al. for a primary tensile strength that corresponds to 1/10 of the material's strength in compression, a typical value for masonry [11].

| Elastic Behavior Parameters | | | | |
|---|---|---|---|---|
| Young's Modulus [GPa] | Density [kg·m$^{-3}$] | Poisson's Ratio [/] | Compressive Strength [MPa] | Tensile Strength [MPa] |
| 3.69 | 1,873 | 0.2 | 6.25 | 0.625 |

Table 1: Material properties for implementation of Maya concrete with CDP.

The postcritical behavior in compression of Maya concrete, expressed as the plot of compressive stress ($\sigma_c$) against total strain ($\varepsilon_{total}$), is derived by scaling the parabolic curve for Roman concrete with the compressive strength of Maya concrete [14] (Figure 9a). Total strain

is converted to inelastic strain ($\varepsilon_{inel}$) for compatibility with the CDP material formulation in Abaqus. The postcritical tensile behavior of Maya concrete is derived using Lourenço's approach [15], modeling tensile stress ($\sigma_t$) as an exponentially decaying function of crack-opening displacement (d) (Figure 9b). The decay rate is calculated as $f_t/G_f$. $G_f$ is the tensile fracture energy 18.125 $N \cdot m^{-1}$, the product of $f_t$ and the tensile ductility index $d_u$ taken as 0.029 mm [11].

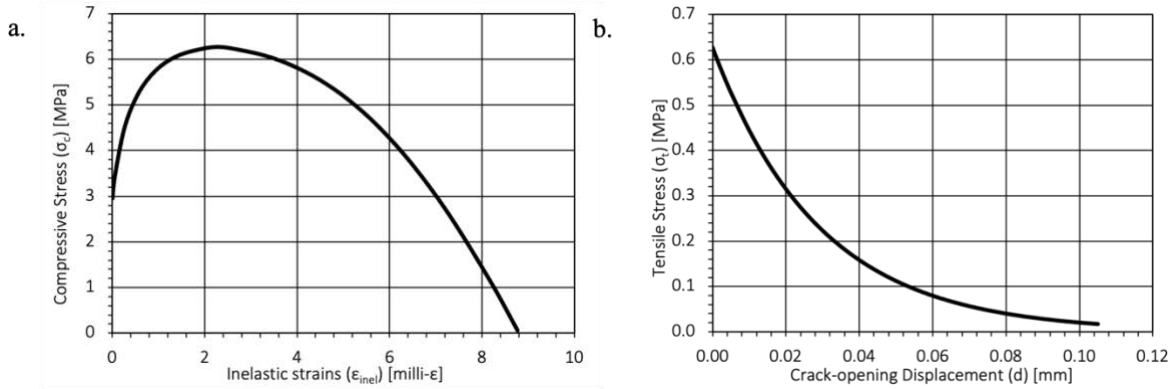


Figure 9: Material definition for Maya concrete in compression (left) and tension (right).

| Plastic Behavior Parameters | | | | |
|---|---|---|---|---|
| Dilation Angle [deg] | Eccentricity [/] | $F_{b0}/f_{c0}$ [/] | K [/] | Viscosity Parameter [/] |
| 31 | 0.1 | 1.16 | 0.67 | 0.0001 |

Table 2: Behavior parameters for implementation of Maya concrete with CDP.

Plastic behavior parameters for the implementation of Concrete Damaged Plasticity (CDP) are adapted from [11][12],[14]-[16]. They are reported in Table 2 above. Given that the tensile strength has not been investigated experimentally but rather is assumed in our research and in previous studies [6], [8], the tensile strength $f_t$ is varied to test the effect of decreasing values of $f_t$ as fractions of $f_c$. The following fractions are considered presently: 1/10, then 1/30, 1/50. Hereafter, the $f_t$ fractions are referred to as F10, F30, F50.

## 2.4 Determination of Failure

The method used to determine a particular failure time of the temples is based on analysis of the time-evolution of energy results and support reactions, both obtained from simulation in Abaqus/CAE Explicit [9]. The energy-based determination of failure was developed in response to the challenges of working with large-scale constructions [8],[17]-[22] and is predicated on a particular feature of the CDP formulation. The usefulness of such a model is illustrated by a 5 m x 5 m x 0.5 m model (Figure 10), the results of which are shown in Figure 11. The example model follows the F10 material formulation described in section 2.3 and the seeding and element type described in section 2.2.

The CDP formulation implemented in the present work uses plastic strains to represent fracture in brittle Maya concrete. Thus, the development of fracture in a model using CDP can be qualitatively tracked by looking at the development of plastic strains. When fractures propagate rapidly at failure, dividing the structure into parts and changing from a static to a dynamic state, the plastic dissipation energy (PD) that accompanies plastic strains propagation grows asymptotically. The point at which PD intersects the strain energy (SE) stored from

loading the structure is taken as the failure point, noted by a vertical line in Figure 11. This is the point at which the structure can no longer sustain the energy imparted to it through loading.

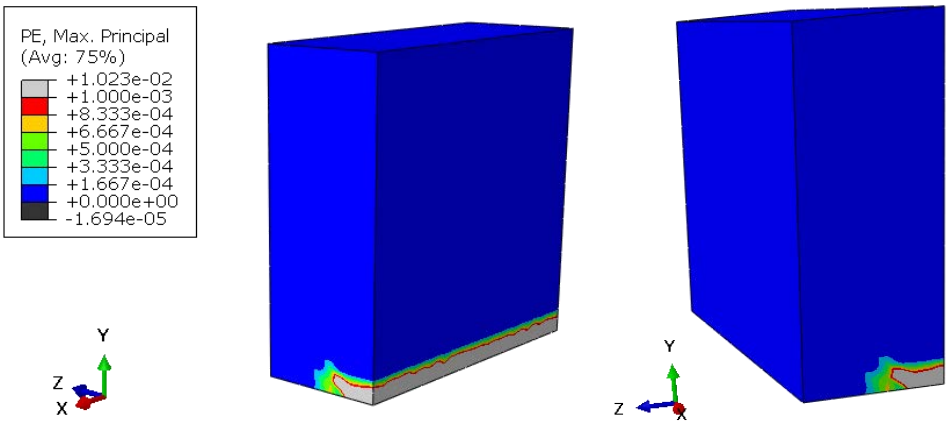


Figure 10: Plastic strain (PE) distribution at failure in a 5x5x0.5 m wall with basal acceleration in the -z direction.

At the same time, support reactions change sharply, signaling that some part of the monument has separated from the base. In the present work, we combine an analysis of support reactions with the energy-based determination of failure illustrated by this section's simple example. Results of the Bonampak temple simulations' reaction and energy outputs, presented below, consistently converge to the same failure time.

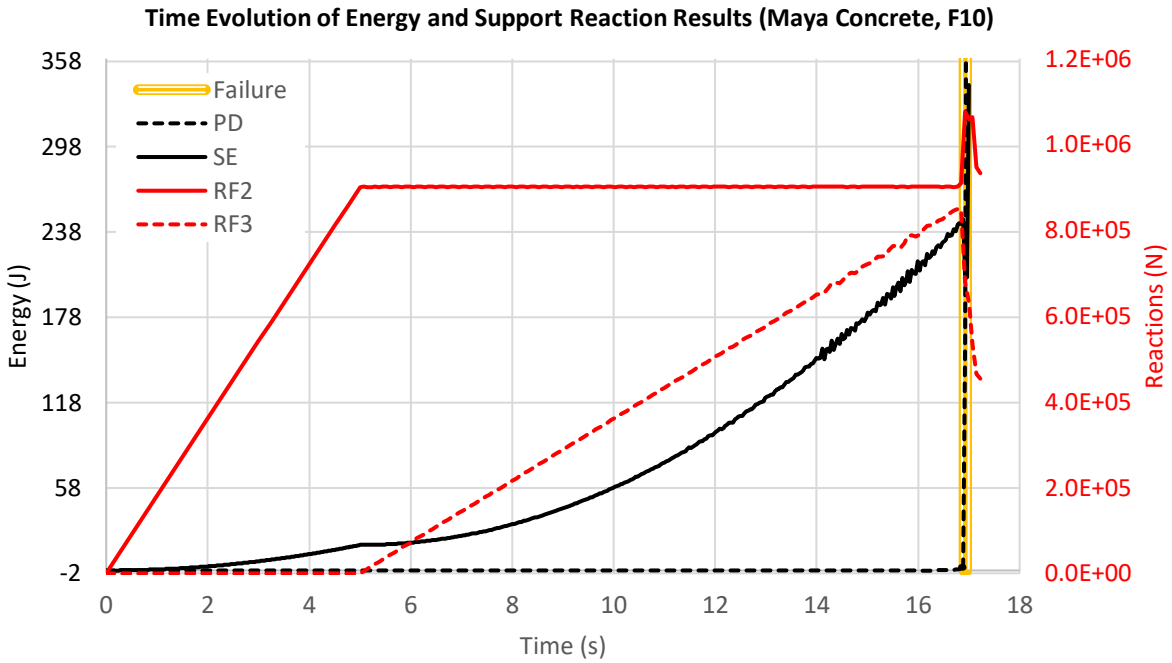


Figure 11: Time evolution of energy (left axis) and support reactions (right axis) for example given above.

## 3 RESULTS

Various configurations of the structures in the presence or absence of inclination and crestería are studied. Pushover analyses were conducted for various tensile strengths with unilateral accelerations in both North-South (NS), and East-West (EW) directions.

### 3.1 Structure 3

Structure 3 shows signs of crestería when it was built. In this paper, the configuration of Structure 3 that includes a crestería is considered the original state. Structure 3 in its present state shows that crestería has collapsed. It is not known whether the structure tilted before or after its collapse, thus we also investigate the configuration of an inclined base in both the assumed original state, with a crestería, and in its extant state, without a crestería.

Table 3 shows lateral capacities $\lambda_c$ of Structure 3 with the presence of a crestería. North-South (NS) acceleration produces higher acceleration capacities compared to East-West (EW) acceleration. All lateral capacities are greater than the peak ground acceleration (PGA) – 0.255g – of the Bonampak, Chiapas area [7].

| | North-South (NS) Acceleration | | East-West (EW) Acceleration | |
|---|---|---|---|---|
| | No Inclination | Inclination | No Inclination | Inclination |
| ft/fc | $\lambda_c$ [g] | $\lambda_c$ [g] | $\lambda_c$ [g] | $\lambda_c$ [g] |
| F10 | 1.04 | 1.00 | 0.74 | 0.80 |
| F30 | 0.72 | 0.54 | 0.40 | 0.43 |
| F50 | 0.51 | 0.41 | 0.29 | 0.32 |

Table 3: Pushover results for Structure 3 with crestería for various tensile formulations.

Table 4 shows lateral capacities $\lambda_c$ of Structure 3 in its present state, without the crestería. Unlike in its original state, the lateral capacities of the present-state Structure 3 are greater when an acceleration is applied in the EW direction as opposed to NS direction.

| | North-South (NS) Acceleration | | East-West (EW) Acceleration | |
|---|---|---|---|---|
| | No Inclination | Inclination | No Inclination | Inclination |
| ft/fc | $\lambda_c$ [g] | $\lambda_c$ [g] | $\lambda_c$ [g] | $\lambda_c$ [g] |
| F10 | 1.29 | 1.17 | - | - |
| F30 | 1.04 | 0.86 | 1.35 | 1.32 |
| F50 | 0.92 | 0.80 | 1.11 | 1.07 |

Table 4: Pushover results for Structure 3 in current state (crestería missing) with various tensile formulations.

Visualizations of plastic strain (PE) in Structure 3 at the instance of failure $\lambda_c$ illustrate zones of greatest risk. An example using an F50 material model is shown in Figure 12, where NS acceleration pushover analysis is shown for Structure 3 in its a) current state, and b) original state. In both models, plastic strain starts to develop in the base of the temple's SW wall.

In Structure 3's original state, the acceleration capacity is lower, and the crestería fails before the temple building itself. This is true for the model of Structure 3's original state under both acceleration scenarios: the crestería collapses first in both the NS loading case (Figure 12b) and the EW loading case (Figure 13b). Under EW acceleration (Figure 13), the original configuration does not show plastic strain development in the temple at all. The lateral capacity of the current state is 1.07g, well beyond the seismic demand of the region (Figure 13a).

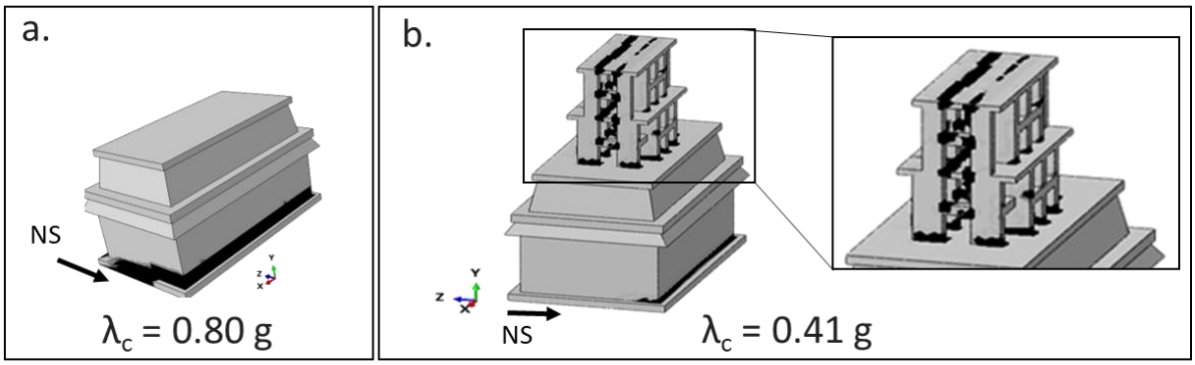


Figure 12: Development of plastic strains produced by NS acceleration, at failure instances with ($\lambda_c$) values taken from inclined Structure 3 of material F50, (a) in its current state $\lambda_c$ = 0.80 g, and (b) with crestería $\lambda_c$ = 0.41 g.

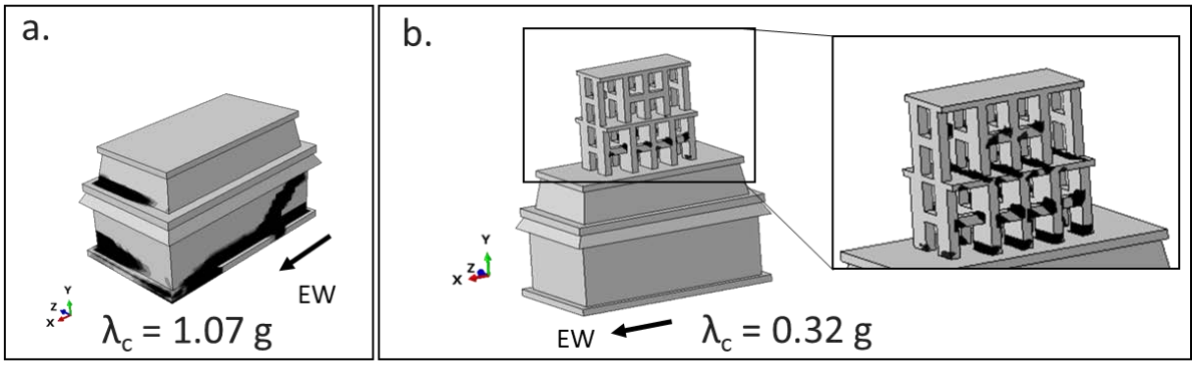


Figure 13: Development of plastic strains produced by EW acceleration, at failure instances with ($\lambda_c$) values taken from inclined Structure 3 of material F50, (a) in its current state $\lambda_c$ = 1.07 g, and (b) with crestería $\lambda_c$ = 0.32 g.

### 3.2 Structure 1

Survey of Structure 1 does not show any evidence of a crestería on the roof of the temple in the past, and its foundation does not have inclination like Structure 3. We thus omit crestería. And the scenario of Structure 1 becoming inclined from the 3D models. The results shown in Table 5 show the lateral capacities derived from models of the current state of Structure 1.

| | North-South (NS) Acceleration | East-West (EW) Acceleration |
|---|---|---|
| ft/fc | $\lambda_c$ [g] | $\lambda_c$ [g] |
| F10 | 0.99 | 1.92 |
| F30 | 0.64 | 1.23 |
| F50 | 0.55 | 1.02 |

Table 5: Pushover results for Structure 1 with various tensile formulations.

For NS acceleration, plastic strain develops predominantly on Structure 1's SW wall, creating a fracture that propagates to the front of the temple, as shown in an F50 material example in Figure 14c. Fracture propagation is similar to Structure 3 as shown in Figure 12. In the EW direction, plastic strain development occurs on bottom-west side of Structure 1 (Figure 15).

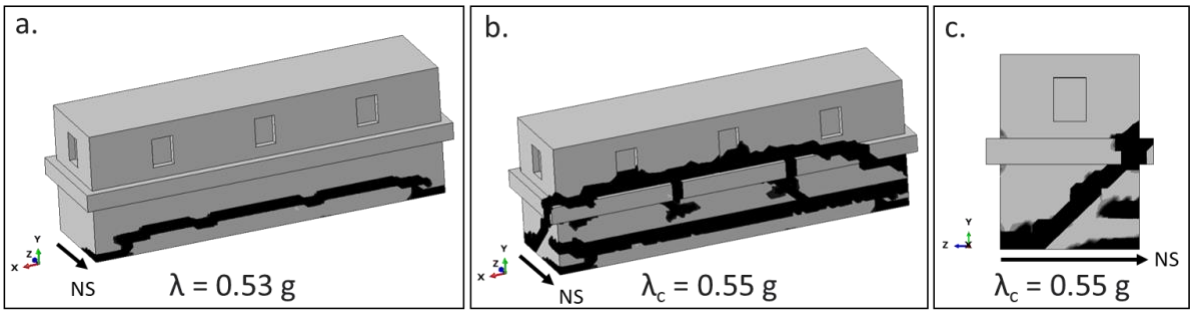


Figure 14: Development of plastic strain under NS acceleration at (a) normalized basal shear (λ) value λ = 0.53g, (b) failure instance of $\lambda_c$ = 0.55g and (c) $\lambda_c$ side view. Results from current state of Structure 1 of material F50.

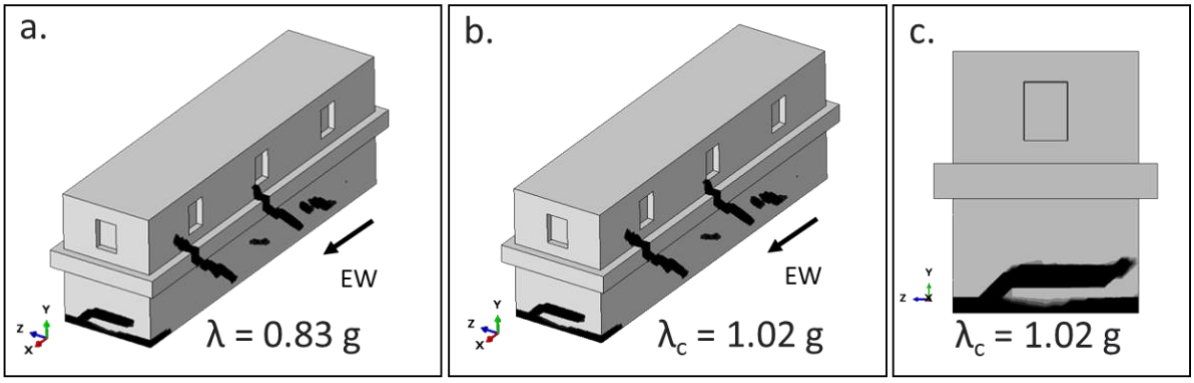


Figure 15: Development of plastic strain under EW acceleration at (a) normalized basal shear (λ) value λ = 0.83g, (b) failure instance of $\lambda_c$ = 1.02g, and (c) $\lambda_c$ side view. Results from current state of Structure 1 of material F50.

### 3.3 Comparison of Structures

We further analyze the results of the current states of both Structure 1 and Structure 3 to investigate their vulnerability to seismic action in the Bonampak, Chiapas area. Compared to the peak ground acceleration demand for the area, the lateral capacities of both structures are much higher (Figure 16).

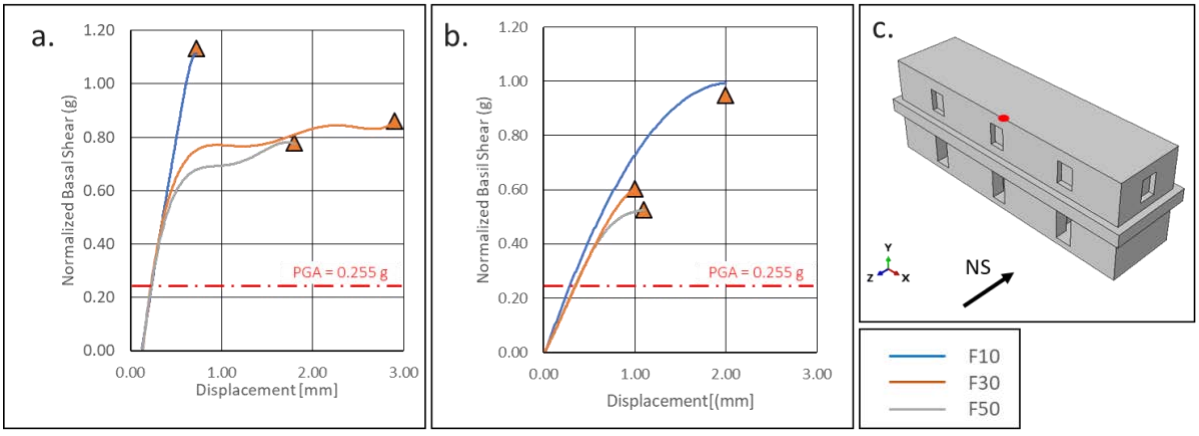


Figure 16: Lateral capacity curve produced by NS ground acceleration applied to the current states of a) Structure 3 b) Structure 1, for various tensile formulations. The relative displacement in the curves is obtained from node shown in c).

Our results yield lateral capacities for Structure 3 (Figure 16a) that are greater than those of Structure 1 (Figure 16b) for corresponding tensile strengths. For both structures, the identified lateral capacity is lower for lower tensile strengths. The relative displacement shown in the horizontal axes of Figure 16a and Figure 16b is obtained from the nodes highlighted at the center of the base and roof of each structure (Figure 16c).

## 4 DISCUSSION

The seismic demand for the Bonampak, Chiapas area is 0.255g [7], well below the lateral capacities reported in section 3 (Figure 16). All models with tensile strengths greater than F50 – 1/50 of the compressive strength of the Maya concrete, which is five times less than the civil engineering standard for basic tensile strength on masonry materials [11] – exceed the seismic demand for the Bonampak region.

The lowest lateral capacity identified (0.55g) occurs when a North-South (NS) acceleration is applied to Structure 1 in its current state using material F50 (Table 5). It is worth noting that there are configurations with lower lateral capacities of 0.52g and 0.43g, which are, the NS acceleration and the EW acceleration for inclined Structure 1. We do not use either of the configurations to draw the conclusion of the structural integrity of Structure 1 because they are hypothetical. However, monitoring the inclination of the base of Structure 1 may be advisable.

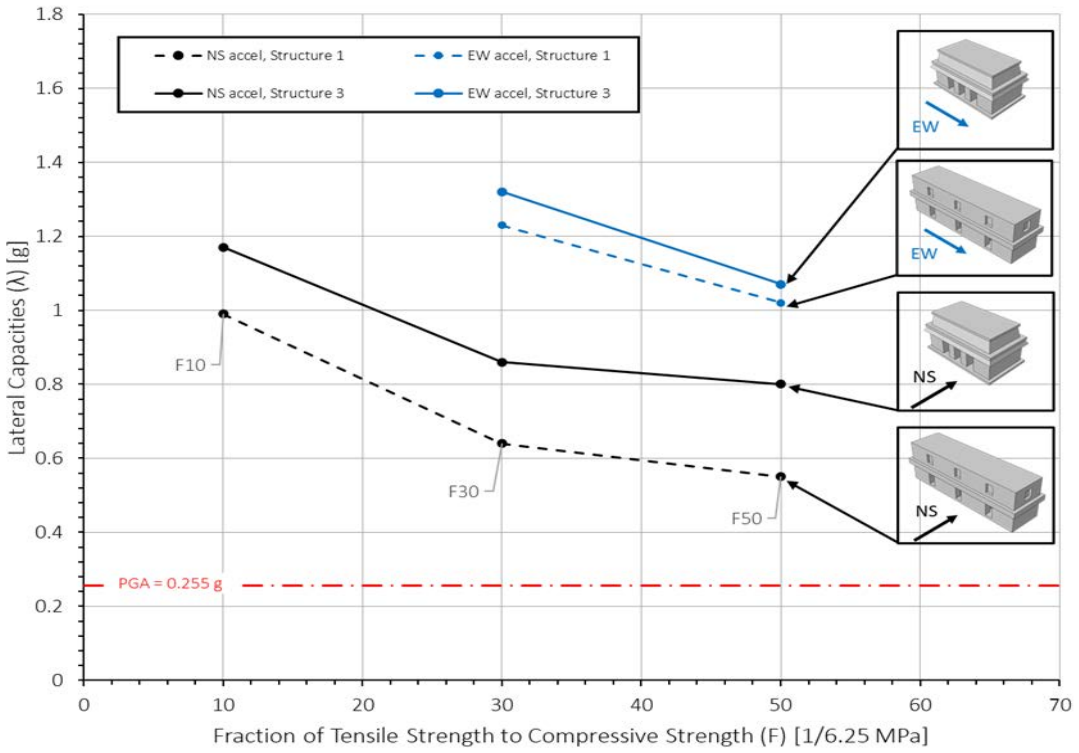


Figure 17: Decreasing tensile strength vs. lateral capacity for models of the present state of Structure 1 (non-inclined) and Structure 3 (inclined).

Figure 17 shows the overview of the lateral capacities of both structures in their current states for NS and EW accelerations. These results confirm the preliminary discussion in [8] that a sectional model underestimates the lateral capacity, when compared with full 3D models (Figure 18). Sectional models lack shear-resistant bounding walls that offer support under lateral accelerations. It is also worth noting that both structures are relatively vulnerable (have

lower lateral capacities) under NS (black) pushover analysis as compared to EW (blue) pushover analysis.

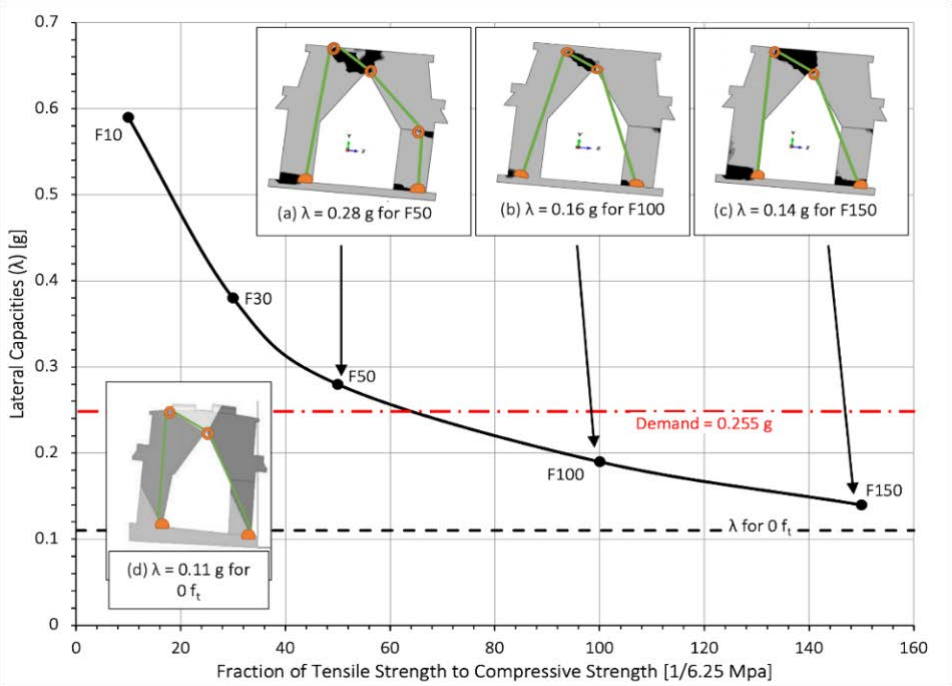


Figure 18: Pushover lateral capacity with failure mechanisms for sectional models with tensile strength fractions: (a) F50, (b) F100, (c) F150, and (d) Flores and Orea's kinematic limit analysis [6].

Convergence to the results presented by Flores and Orea [6] is observed in our preliminary results [8] as the tensile strength of Maya concrete is decreased (Figure 18). Based on the results illustrated in Figure 17, convergence is again demonstrated with the present models under discussion.

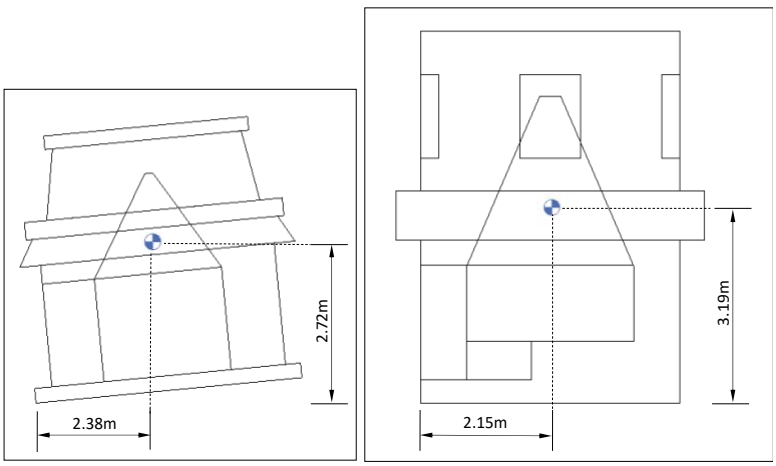


Figure 19: Position of center of mass for Structure 3 (left, with dashed lines) and Structure 1 (right). Due to symmetry, the position of the center of mass is midway along the length dimension.

A comparison of the lateral capacity values of Structures 1 and 3 predicts that Structure 1 would fail under consistently lower lateral accelerations than Structure 3. This can be explained by Structure 1's relatively higher center of gravity (Figure 19). The higher center of mass

produces a more unstable equilibrium, which makes it more sensitive to external effects (i.e. seismic loading) being applied.

Under North-South (NS) accelerations, the lateral capacities of all inclined configurations are lower than their non-inclined counterparts. Inclined configurations all show evidence of toppling down the incline due to the fracture that develops from the base of the back side of the structures (Figure 12, Figure 14), a finding that confirms our previous work for bounded 3D sectional models of Structure 3 in its present state [8].

## 5 CONCLUSIONS AND FUTURE WORK

The most conservative Structure 3 models of the present work, which have a tensile strength as low as 1/50 of compressive strength (F50) of Maya concrete, produce lateral capacities that range from 0.80 g to 1.17 g with applied North-South (NS) acceleration. Additionally, the lateral capacity is at least 1.07 g with applied East-West (EW) acceleration. Similarly, the lateral capacity of present state Structure 1 varies from 0.55 g to 0.99 g with applied NS acceleration, and at least 1.02 g with applied EW acceleration.

These data suggest that all structures exceed the known seismic demand for the Bonampak area, 0.255g. The most vulnerable of all configurations studied is Structure 1 in its current state, with NS acceleration applied. This produces a lateral capacity of 0.55g, which exceeds the seismic demand by a factor of 2.2. According to the present research, both structures will remain structurally integral when up to seismic acceleration as high as 0.255g is applied.

In the future, a time history analysis based on the application of an appropriate seismic signal should be performed on the two structures. All future research should emphasize Structure 1, since the present work shows that it is more vulnerable than Structure 3.

## REFERENCES

[1] J. Thompson, T. Proskouriakoff, K. Ruppert, *Bonampak, Chiapas, Mexico*, Washington, D.C.: Carnegie Institution of Washington; 1955.

[2] B. Dupont, Temples of the Murals, Bonampak, Chiapas, MEXICO. Taken on February 13, 2020. https://www.flickr.com/photos/berniedup/49533952222/in/photostream/. Accessed February 2023.

[3] L. Roys, *Engineering knowledge of the Maya*, Washington, D.C.: Carnegie Institute; 1934.

[4] Peabody Museum of Archaeology and Ethnology, *Structure 3. West end.* 17 October 1955. https://library.artstor.org/#/asset/AHARVARD_10310419961. Accessed October 10, 2021.

[5] B. Dupont, *Structure N° 3*; 13 February 2020. https://www.flickr.com/photos/berniedup/49533819162/. Accessed October 2021.

[6] C. Flores Espino, H. Orea Magaña, Vulnerability analysis of two Mayan vaulted structures aided by a genetic algorithm tool. K. Van Balen, E. Verstrynge eds. *10th International Conference on Structural Analysis of Historical Constructions (SAHC 2016),* Leuven, Belgium, September 13-15, 978-985, 2016.

[7] A. Rodríguez-Lomelí, J. García-Mayordomo, Seismic hazard at a triple plate junction: the state of Chiapas (México). *Natural Hazards*, 97(3), 1297-1325, 2019. doi:10.1007/s11069-019-03710-4.

[8] O. Hamad, J. Sennyondo, H. Kimanya, D. Nguyen, S. Tezcan, R. Perucchio, Structural Assessment of Concrete Vaulted Maya Temples of Bonampak, Chiapas, Mexico. I. Lombillo, M. Paz Saez eds. *9th EuroAmerican Congress on Construction Pathology, Rehabilitation Technology and Heritage Management (REHABEND 2022)*, Granada, Spain, September 13-16, 2022.

[9] Dassault Systems SIMULIA – Abaqus (2020).

[10] R. Pinho, Using pushover analysis for assessment of buildings and bridges. A. Pecker ed. *Advanced Earthquake Engineering Analysis*, 494, 91-120, 2007.

[11] M. Angelillo, G. Milani, P. Lourenço, Masonry behaviour and modelling. *Mechanics of Masonry Structures*, 1-26, 2014.

[12] H. Ramírez de Alba, E. Valdez Medina, Cementitious materials and concrete of ancient cultures in America and Yaxchilan bridge. P. Roca, P. Lourenço, C. Modena eds. *9th International Conference on Structural Analysis of Historical Constructions, (SAHC 2014),* Mexico City, Mexico, October 14-17, 2014.

[13] H. Coutiño, *Estudio del Concreto Maya.* PhD Dissertation, Universidad Autónoma del Estado de México, 2000. [In Spanish]

[14] P. Brune P. *The mechanics of imperial roman concrete and the structural design of vaulted monuments*. Ph.D. Dissertation, University of Rochester, 2010.

[15] P. Lourenço, *Computational Strategies for Masonry Structures.* PhD thesis, Delft University, 1996.

[16] N. Tarque, *Numerical modelling of the seismic behavior of adobe building*. PhD dissertation, Universitá degli Studi di Pavia, Italy, 2011.

[17] S. Tezcan, N. Tambe, C. Muir, R. Aguilar, R. Perucchio, Nonlinear FE Analysis of the Response to Lateral Accelerations of the Triumphal Arch of the Church of Andahuaylillas, Peru. *11th International Conference on Structural Analysis of Historical Constructions (SAHC 2018),* Cusco, Peru, September 11-13, 2018.

[18] S. Tezcan, M.A. Pando, R. Aguilar, B. Castañeda, C. Rojas, R. Perucchio, Preliminary nonlinear static and dynamic analysis of the main pyramid of Huaca de la Luna, Peru. P. Roca, L. Pela, C. Molins eds. *8th International Conference on Computational Methods in Structural Dynamics and Earthquake Engineering (COMPDYN 2021),* online, June 28-30, 2021. https://doi.org/10.7712/120121.8478.18791.

[19] J. Sun, S. Tezcan, R. Perucchio, The structural function of the Dutch buttressing of the east curtain wall of Elmina Castle, Elmina, Ghana. Roca, P., Pela, L., Molins, C. eds. *12th International Conference on Structural Analysis of Historical Constructions (SAHC 2021)*, online, September 29-October 01, 2021.

[20] F. Faleri, N. Grillanda, S. Tezcan, R. Perucchio, G. Milani, Role of repeated seismic events on the collapse of two calidaria in Rome dating back to Imperial age. *8th International Conference on Computational Methods in Structural Dynamics and Earthquake Engineering (COMPDYN 2021),* online, June 28-30, pp. 406-414, 2021.

[21] A. Remus, L. Yilmaz, S. Tezcan, R. Perucchio, Effect of eastern architecture and sloping foundation conditions on the structural response of the adobe pyramid Huaca de la Luna (Perú). Y. Endo, T. Hanazato eds. *13th International Conference on Structural Analysis of Historical Constructions (SAHC 2023)* Kyoto, Japan, September 13-15, 2023.

[22] S. Tezcan, M. Pando, R. Aguilar, R. Perucchio, Nonlinear 2D and 3D Finite Element Static, Dynamic and Time History Analysis of the Main Pyramid of Huaca de la Luna, Peru. Y. Endo, T. Hanazato eds. *13th International Conference on Structural Analysis of Historical Constructions (SAHC 2023)*, Kyoto, Japan, September 13-15, 2023.